

# LHC constraints on gauge boson couplings to dark matter

Andreas Crivellin,<sup>1,\*</sup> Ulrich Haisch,<sup>2,1,†</sup> and Anthony Hibbs<sup>2,‡</sup>

<sup>1</sup>*CERN Theory Division, CH-1211 Geneva 23, Switzerland*

<sup>2</sup>*Rudolf Peierls Centre for Theoretical Physics, University of Oxford, OX1 3PN Oxford, United Kingdom*

(Dated: November 13, 2018)

Collider searches for energetic particles recoiling against missing transverse energy ( $\cancel{E}_T$ ) allow to place strong bounds on the interactions between dark matter (DM) and standard model (SM) particles. In this article we update and extend LHC constraints on effective dimension-7 operators involving DM and electroweak gauge bosons. A concise comparison of the sensitivity of the mono-photon, mono- $W$ , mono- $Z$ , mono- $W/Z$ , invisible Higgs-boson decays in the vector boson fusion (VBF) mode and the mono-jet channel is presented. Depending on the parameter choices, either the mono-photon or the mono-jet data provide the most stringent bounds at the moment. We furthermore explore the potential of improving the current 8 TeV limits at 14 TeV. Future strategies capable of disentangling the effects of the different effective operators involving electroweak gauge bosons are discussed as well.

## I. INTRODUCTION

Because of their potential connection to DM, searches for  $\cancel{E}_T$  represent one of the main lines of LHC research. These searches can be categorised based on the type of SM particles that recoil against DM. By now, ATLAS and CMS have considered a plethora of different final states in DM searches containing jets of hadrons, gauge bosons, heavy quarks and even the Higgs boson (see e.g. [1] for a recent review of the experimental status).

In most cases these studies are performed in the context of an effective field theory (EFT) which correctly captures the physics of heavy particles mediating the interactions between DM and SM fields, if the mediators are heavy enough to be integrated out. Below we will consider the effective Lagrangian

$$\mathcal{L}_{\text{eff}} = \sum_{k=B,W,\tilde{B},\tilde{W}} \frac{C_k(\mu)}{\Lambda^3} O_k, \quad (1)$$

which contains the following four  $SU(2)_L \times U(1)_Y$  gauge-invariant dimension-7 operators

$$\begin{aligned} O_B &= \bar{\chi}\chi B_{\mu\nu}B^{\mu\nu}, & O_W &= \bar{\chi}\chi W_{\mu\nu}^i W^{i,\mu\nu}, \\ O_{\tilde{B}} &= \bar{\chi}\chi B_{\mu\nu}\tilde{B}^{\mu\nu}, & O_{\tilde{W}} &= \bar{\chi}\chi W_{\mu\nu}^i \tilde{W}^{i,\mu\nu}. \end{aligned} \quad (2)$$

Here  $\Lambda$  represents the scale of new physics at which the higher-dimensional operators (1) are generated, i.e. the scale where the messenger particles are removed as active degrees of freedom. The DM particle  $\chi$  can be both a Dirac or a Majorana fermion and  $B_{\mu\nu} = \partial_\mu B_\nu - \partial_\nu B_\mu$  ( $W_{\mu\nu}^i = \partial_\mu W_\nu^i - \partial_\nu W_\mu^i + g_2 \epsilon^{ijk} W_\mu^j W_\nu^k$ ) is the  $U(1)_Y$  ( $SU(2)_L$ ) field strength tensor, while  $\tilde{B}_{\mu\nu} = 1/2 \epsilon_{\mu\nu\lambda\rho} B^{\lambda\rho}$  ( $\tilde{W}_{\mu\nu}^i = 1/2 \epsilon_{\mu\nu\lambda\rho} W^{i,\lambda\rho}$ ) denotes its dual and  $g_2$  is the weak coupling constant.

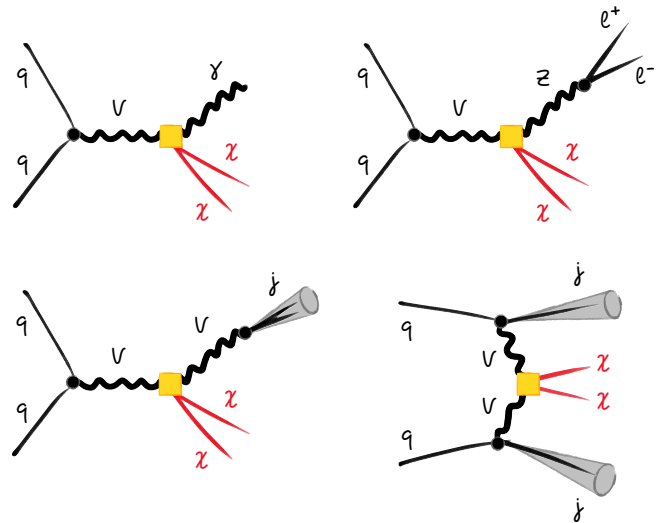


FIG. 1: Representative examples of graphs that generate a  $\cancel{E}_T + \gamma$ ,  $\cancel{E}_T + Z$  ( $\rightarrow \ell^+ \ell^-$ ),  $\cancel{E}_T + W/Z$  ( $\rightarrow j$ ) or a  $\cancel{E}_T + 2j$  signal. The operator insertions are indicated by yellow squares while SM vertices are represented by black dots. Propagators labeled by  $V$  include all possible photon,  $Z$ -boson or  $W$ -boson exchanges. See text for further details.

The operators introduced in (2) appear in models of Rayleigh DM (see for instance [2–4]). They are special in the sense that, up to dimension 7, they are the only effective interactions which lead to velocity-suppressed annihilation rates of DM to photon pairs [5–7]. While the sensitivity of future direct detection experiments may allow to set novel bounds on the Wilson coefficients  $C_B(\Lambda)$  and  $C_W(\Lambda)$  for heavy DM particles with  $m_\chi \gtrsim 1$  TeV once loop effects are taken into account [8], in the case of light DM the leading (and for  $C_{\tilde{B}}(\Lambda)$  and  $C_{\tilde{W}}(\Lambda)$  the only) restrictions arise and will continue to arise from collider searches involving large amounts of  $\cancel{E}_T$ . In fact, the DM-SM interactions (2) have been constrained using 7 TeV and 8 TeV LHC data on invisible decays of the

\*Electronic address: andreas.crivellin@cern.ch

†Electronic address: u.haisch1@physics.ox.ac.uk

‡Electronic address: Anthony.Hibbs@physics.ox.ac.uk

Higgs boson in the VBF mode [9] as well as the  $\cancel{E}_T + Z$  [10, 11], the mono-photon [12] and the  $\cancel{E}_T + W$  [13] channel.

The main goal of this article is twofold. First, to update the existing constraints by taking into account the latest mono-photon [14, 15],  $\cancel{E}_T + W/Z$  ( $\rightarrow$  hadrons) [16] and VBF  $h \rightarrow$  invisible [17] searches. Second, to extend the studies [9–13] by considering in addition the  $\cancel{E}_T + W$  ( $\rightarrow$  leptons) channel [18, 19] as well as the newest mono-jet data [20]. An assortment of Feynman diagrams that lead to the  $\cancel{E}_T$  signatures investigated in the following are displayed in Fig. 1.

Our analysis shows that depending on the choice of parameters, either the mono-photon or the mono-jet data give rise to the strongest restrictions at present. By combining the information on all available channels we are thus able to derive bounds on the coefficients  $C_k(\Lambda)/\Lambda^3$  in (1) that improve on the existing limits. Building upon [21], we furthermore demonstrate that measurements of the jet-jet azimuthal angle difference in  $\cancel{E}_T + 2j$  events may be used to disentangle whether the DM bilinear  $\bar{\chi}\chi$  couples more strongly to the combination  $B_{\mu\nu}B^{\mu\nu}$  ( $W_{\mu\nu}^i W^{i,\mu\nu}$ ) or the product  $B_{\mu\nu}\tilde{B}^{\mu\nu}$  ( $W_{\mu\nu}^i \tilde{W}^{i,\mu\nu}$ ) of field strength tensors. Similar ideas have also been brought forward in [9].

The outline of this article is as follows. In Sec. II we review the existing LHC searches for  $\cancel{E}_T$  signatures that we will use to constrain the effective interactions (2). In Sec. III we derive the restrictions on the parameter space by combining all individual search modes, commenting also on how future measurements may improve these limits. This section contains in addition a discussion of the azimuthal angle correlations between the two jets in the  $\cancel{E}_T + 2j$  channel. Our conclusions are presented in Sec. IV.

## II. SEARCH CHANNELS

In this section we list the various cuts and the values of the fiducial cross section ( $\sigma_{\text{fid}}$ ) of each individual  $\cancel{E}_T$  channel. This information will be used in the next section to set limits on the coefficients  $C_k(\Lambda)/\Lambda^3$  appearing in the effective Lagrangian (1).

### A. Mono-photon signal

We begin with the mono-photon signal, which has recently been searched for by both CMS [14] and ATLAS [15]. Since the former search leads to the stronger restrictions, we employ the CMS results, which are based on  $19.6 \text{ fb}^{-1}$  of 8 TeV data. The relevant cuts are

$$\cancel{E}_T > 140 \text{ GeV}, \quad |\eta_\gamma| < 1.4442, \quad (3)$$

where  $\eta_\gamma$  denotes the pseudorapidity of the photon. The CMS collaboration performs the measurement in six dif-

ferent signal regions with a varying cut on the transverse momentum of the photon ( $p_{T,\gamma}$ ). Note that due to the higher-dimensional nature of the operators (2), the  $\cancel{E}_T + \gamma$  signal has a rather hard  $p_{T,\gamma}$  spectrum. As a result, we find that the most severe cut of  $p_{T,\gamma} > 700 \text{ GeV}$  gives the strongest bounds on the parameter space in our case. The corresponding 95% confidence level (CL) limit on the fiducial cross section reads

$$\sigma_{\text{fid}}(pp \rightarrow \cancel{E}_T + \gamma) < 0.22 \text{ fb}. \quad (4)$$

### B. Mono-Z signal

In the case of the  $\cancel{E}_T + Z$  ( $\rightarrow \ell^+\ell^-$ ) search channel, we use the ATLAS results [11], that utilise  $20.3 \text{ fb}^{-1}$  of 8 TeV data. The selection criteria relevant to our analysis are

$$p_{T,\ell} > 20 \text{ GeV}, \quad |\eta_\ell| < 2.5, \quad m_{\ell\ell} \in [76, 106] \text{ GeV},$$

$$|\eta_{\ell\ell}| < 2.5, \quad \frac{|p_{T,\ell\ell} - \cancel{E}_T|}{p_{T,\ell\ell}} < 0.5. \quad (5)$$

Here  $m_{\ell\ell}$ ,  $\eta_{\ell\ell}$  and  $p_{T,\ell\ell}$  denote the invariant mass, the pseudorapidity and the transverse momentum of the dilepton system, respectively. The ATLAS analysis defines four signal regions with different lower  $\cancel{E}_T$  thresholds. As it turns out, in the considered case the requirement  $\cancel{E}_T > 350 \text{ GeV}$  gives rise to the best bounds. Including  $Z$ -boson decays to both electrons and muons ( $\ell = e, \mu$ ), the ATLAS experiment obtains for this  $\cancel{E}_T$  cut the following 95% CL bound

$$\sigma_{\text{fid}}(pp \rightarrow \cancel{E}_T + Z (\rightarrow \ell^+\ell^-)) < 0.27 \text{ fb}. \quad (6)$$

### C. Mono-W signal

Both ATLAS [18] and CMS [19] have searched for a mono- $W$  signal in the leptonic decay mode. We find that the ATLAS search for the  $\mu\nu_\mu$  final state, which uses  $20.3 \text{ fb}^{-1}$  of 8 TeV data, gives the strongest constraints, and thus we consider only this channel. The most important experimental cuts are

$$p_{T,\mu} > 45 \text{ GeV}, \quad |\eta_\mu| \in [0, 1] \cup [1.3, 2],$$

$$m_T = \sqrt{2p_{T,\mu}\cancel{E}_T(1 - \cos\varphi_{\mu\cancel{E}_T})}, \quad (7)$$

where  $m_T$  is the transverse mass which depends on the angle  $\varphi_{\mu\cancel{E}_T}$  between the  $p_{T,\mu}$  and the  $\cancel{E}_T$  vectors. ATLAS sets bounds on  $\sigma_{\text{fid}}$  for three different  $m_T$  cuts, and like in the case of the mono-photon signal, we observe that the strongest restriction of  $m_T > 843 \text{ GeV}$  provides the best limits on the interactions (2). At 95% CL the bound on the corresponding fiducial signal cross section is given by

$$\sigma_{\text{fid}}(pp \rightarrow \cancel{E}_T + W (\rightarrow \mu\nu_\mu)) < 0.54 \text{ fb}. \quad (8)$$

### D. Mono- $W/Z$ signal

The ATLAS search [16] looks for a  $\cancel{E}_T + W/Z$  signal, where the  $W$  or  $Z$  boson decays hadronically. This analysis is based on  $20.3 \text{ fb}^{-1}$  of 8 TeV data, jet candidates are reconstructed using the Cambridge/Aachen (C/A) algorithm [22] with a radius parameter  $R = 1.2$  and subjected to a mass-drop filtering procedure [23]. Events are required to have at least one C/A jet with

$$\begin{aligned} p_{T,j} &> 250 \text{ GeV}, & |\eta_j| &< 1.2, \\ m_j &\in [50, 120] \text{ GeV}, & \sqrt{y} &> 0.4. \end{aligned} \quad (9)$$

Here  $m_j$  refers to the mass of the large-radius jet, while  $\sqrt{y} = \min(p_{T,j_1}, p_{T,j_2}) \sqrt{(\Delta\phi_{j_1 j_2})^2 + (\Delta\eta_{j_1 j_2})^2} / m_j$  is a measure of the momentum balance of the two leading subjects  $j_1$  and  $j_2$  contained in the C/A jet. The 95% CL limits on the fiducial cross section depend also on the imposed  $\cancel{E}_T$  threshold, and it turns out that the stronger of the two cuts, i.e.  $\cancel{E}_T > 500 \text{ GeV}$ , provides the most stringent constraints. In this case, the relevant limit on the fiducial cross section is

$$\sigma_{\text{fid}}(pp \rightarrow \cancel{E}_T + W/Z (\rightarrow \text{hadrons})) < 2.2 \text{ fb}. \quad (10)$$

### E. Mono-jet signal

One can also use mono-jet events to constrain the operators in (2), since the corresponding searches allow for the presence of a secondary jet. Here we will employ the newest CMS results [20], which make use of  $19.7 \text{ fb}^{-1}$  of 8 TeV data. Like CMS, we reconstruct jets using an anti- $k_t$  algorithm [24] with radius parameter  $R = 0.5$ . The relevant selection cuts are

$$\begin{aligned} p_{T,j_1} &> 110 \text{ GeV}, & |\eta_{j_1}| &< 2.4, \\ p_{T,j_2} &> 30 \text{ GeV}, & |\eta_{j_2}| &< 4.5, \\ \Delta\phi_{j_1 j_2} &< 2.5, \end{aligned} \quad (11)$$

where  $\Delta\phi_{j_1 j_2}$  is the azimuthal separation of the two leading jets. Another important selection criterion is the imposed jet-veto [26], which rejects events if they contain a tertiary jet with  $p_{T,j_3} > 30 \text{ GeV}$  and  $|\eta_{j_3}| < 4.5$ . The CMS measurement is performed for seven different  $\cancel{E}_T$  regions, and we find that for the considered interactions the highest sensitivity is obtained for  $\cancel{E}_T > 500 \text{ GeV}$ . The corresponding 95% CL limit on the fiducial cross section reads

$$\sigma_{\text{fid}}(pp \rightarrow \cancel{E}_T + 2j) < 6.1 \text{ fb}. \quad (12)$$

### F. VBF invisible Higgs-boson decays

Last but not least, we consider the results of the CMS search for invisible decays of the Higgs boson in the VBF

channel [17], which uses a 8 TeV data sample, corresponding to an integrated luminosity of  $19.5 \text{ fb}^{-1}$ . Jets are reconstructed employing an anti- $k_t$  clustering algorithm with  $R = 0.5$ , and subject to the following requirements

$$\begin{aligned} p_{T,j_1}, p_{T,j_2} &> 50 \text{ GeV}, & |\eta_{j_1}|, |\eta_{j_2}| &< 4.7, \\ \eta_{j_1} \cdot \eta_{j_2} &< 0, & \Delta\eta_{j_1 j_2} &> 4.2, \\ m_{j_1 j_2} &> 1100 \text{ GeV}, & \Delta\phi_{j_1 j_2} &< 1.0. \end{aligned} \quad (13)$$

The missing-energy cut is  $\cancel{E}_T > 130 \text{ GeV}$  and a central jet-veto is imposed to any event that has a third jet with  $p_{T,j_3} > 30 \text{ GeV}$  and a pseudorapidity between those of the two tagging jets. For these cuts, CMS obtains the following 95% CL bound on the fiducial cross section

$$\sigma_{\text{fid}}(pp \rightarrow \cancel{E}_T + 2j) < 6.5 \text{ fb}. \quad (14)$$

## III. NUMERICAL RESULTS

In order to determine the cross section for the  $\cancel{E}_T$  signals associated to the effective operators (2), we have implemented each of them in FeynRules [27], generating a UFO output [28]. The actual event generation has been performed at leading order with MadGraph 5 [29] utilising CTEQ6L1 parton distributions [30]. Parton-shower effects and hadronisation corrections have been included by means of PYTHIA 8 [31] and jets constructed using FastJet 3 [32]. We employ Delphes 3 [25] as a fast detector simulation to estimate the reconstruction efficiencies for the different  $\cancel{E}_T$  signals. The efficiencies that we find amount to around 70% for the mono-photon signal, 60% in both the mono- $Z$  and mono- $W$  case and 65% for the mono- $W/Z$  signature. These findings agree with [15] for the  $\cancel{E}_T + \gamma$ , [11] for the  $\cancel{E}_T + Z$ , [13] for the  $\cancel{E}_T + W$  and [16] for the  $\cancel{E}_T + W/Z$  signal. For the mono-jet signal and the search for invisible decays of the Higgs boson in the VBF channel, we find reconstruction efficiencies in the ballpark of 95%.

Our Monte Carlo (MC) implementation has been validated by reproducing the numerical results of [11, 12] within theoretical uncertainties. These errors have been assessed by studying the scale ambiguities of our results. We have used the default dynamical scale choice of MadGraph 5, varying the scale factor in the range  $[1/2, 2]$ . We find that the predictions for the mono-photon,  $\cancel{E}_T + Z (\rightarrow \ell^+ \ell^-)$  and  $\cancel{E}_T + W (\rightarrow \mu\nu_\mu)$  cross sections calculated in this way vary by around  $\pm 15\%$ , while in the case of the  $\cancel{E}_T + W/Z (\rightarrow \text{hadrons})$ , the mono-jet and the VBF  $h \rightarrow \text{invisible}$  signal, relative differences of about  $\pm 20\%$  are obtained. Note that these errors are smaller than those found in [26, 33–35], since all the tree-level  $\cancel{E}_T$  cross sections considered in our work do not explicitly depend on  $\alpha_s$ . The quoted uncertainties thus reflect only the ambiguities related to the change of factorisation scale, but not renormalisation scale.

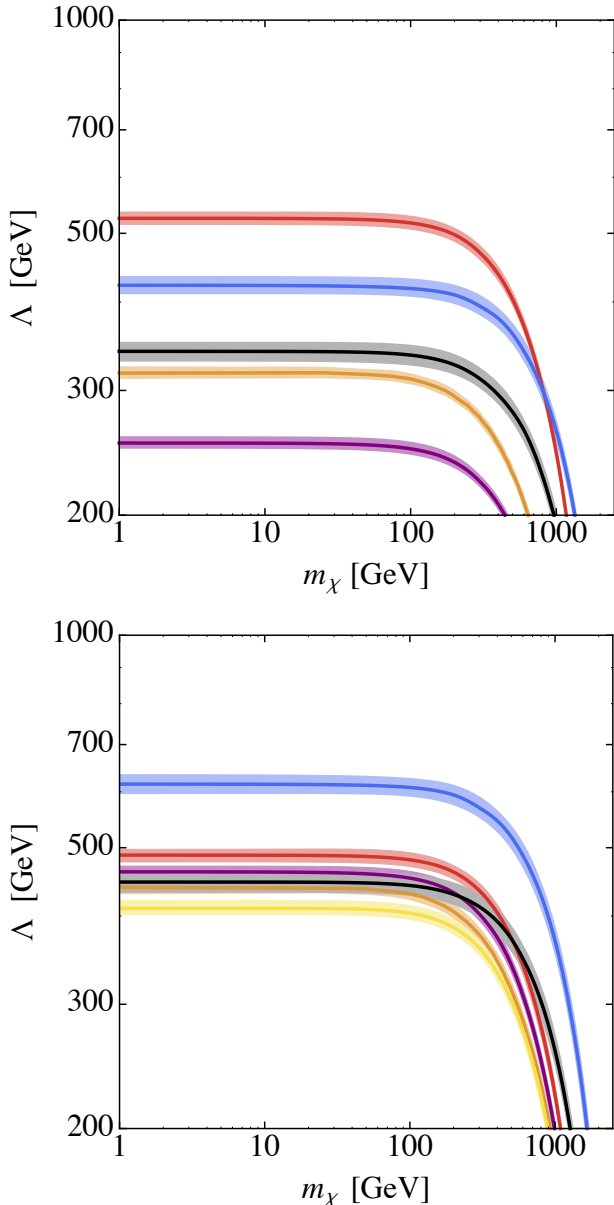


FIG. 2: Assortment of LHC bounds on the new-physics scale  $\Lambda$ , assuming  $C_B(\Lambda) = 1$ ,  $C_W(\Lambda) = 0$  (upper panel) and  $C_B(\Lambda) = 0$ ,  $C_W(\Lambda) = 1$  (lower panel). In both cases the DM particles are taken to be Dirac and  $C_{\tilde{B}}(\Lambda) = C_{\tilde{W}}(\Lambda) = 0$ . The coloured curves correspond to the limits arising from the latest mono-photon (red),  $\cancel{E}_T + Z (\rightarrow \ell^+ \ell^-)$  (orange),  $\cancel{E}_T + W (\rightarrow \mu\nu\mu)$  (yellow),  $\cancel{E}_T + W/Z (\rightarrow \text{hadrons})$  (purple), mono-jet (blue) and VBF  $h \rightarrow \text{invisible}$  (grey) searches. The width of the bands reflect the associated scale uncertainties.

### A. Dependence on a single Wilson coefficient

In Fig. 2 we present the limits on the new-physics scale  $\Lambda$  for  $C_{\tilde{B}}(\Lambda) = C_{\tilde{W}}(\Lambda) = 0$  and the two choices  $C_B(\Lambda) = 1$ ,  $C_W(\Lambda) = 0$  (upper panel) and  $C_B(\Lambda) = 0$ ,  $C_W(\Lambda) = 1$  (lower panel) for the Wilson coefficients eval-

uated at  $\Lambda$ . The shown predictions correspond to Dirac DM and the widths of the coloured bands illustrate the impact of scale variations. For  $C_B(\Lambda) = 1$ ,  $C_W(\Lambda) = 0$ , one observes that the mono-photon search [14] provides the strongest constraints in most of the parameter space. Numerically, we find that the scale  $\Lambda$  has to satisfy  $\Lambda \gtrsim 510$  GeV for  $m_\chi \lesssim 100$  GeV in order to meet the 95% CL requirement (4). In the case  $C_B(\Lambda) = 0$ ,  $C_W(\Lambda) = 1$ , on the other hand, the latest mono-jet data [20] impose the leading restrictions. At 95% CL, the inequality (12) translates into a lower limit of  $\Lambda \gtrsim 600$  GeV for DM masses below 100 GeV. The shown limits also hold in the case that  $C_{\tilde{B}}(\Lambda) = 1$ ,  $C_{\tilde{W}}(\Lambda) = 0$  or  $C_{\tilde{B}}(\Lambda) = 0$ ,  $C_{\tilde{W}}(\Lambda) = 1$  and  $C_B(\Lambda) = C_W(\Lambda) = 0$ , while for Majorana DM the constraints on  $\Lambda$  would be stronger by around 12%. Note finally that  $\cancel{E}_T + W (\rightarrow \mu\nu\mu)$  searches do not provide any constraint on scenarios with  $C_W(\Lambda) = C_{\tilde{W}}(\Lambda) = 0$ .

To better understand the restrictions imposed by the various search channels, we consider the Feynman rules associated to the effective operators  $O_B$  and  $O_W$  entering (1). In momentum space, the resulting interactions between pairs of DM particles and SM gauge bosons take the form

$$\frac{4i}{\Lambda^3} g_{V_1 V_2} (p_1^{\mu_2} p_2^{\mu_1} - g^{\mu_1 \mu_2} p_1 \cdot p_2), \quad (15)$$

where  $p_i$  ( $\mu_i$ ) denotes the momentum (Lorentz index) of the vector field  $V_i$  and for simplicity the spinors associated with the DM fields have been dropped. In terms of the sine ( $s_w$ ) and cosine ( $c_w$ ) of the weak mixing angle and the Wilson coefficients  $C_B(\Lambda)$  and  $C_W(\Lambda)$ , the couplings  $g_{V_i V_j}$  read

$$\begin{aligned} g_{AA} &= c_w^2 C_B(\Lambda) + s_w^2 C_W(\Lambda), \\ g_{AZ} &= -s_w c_w (C_B(\Lambda) - C_W(\Lambda)), \\ g_{ZZ} &= s_w^2 C_B(\Lambda) + c_w^2 C_W(\Lambda), \\ g_{WW} &= C_W(\Lambda). \end{aligned} \quad (16)$$

These results do not coincide with the expressions reported in [10, 12, 13]. From (16) we see that in the coupling  $g_{AA}$  of DM to two photons, the Wilson coefficients  $C_B(\Lambda)$  enters compared to  $C_W(\Lambda)$  with a relative factor of  $c_w^2/s_w^2 \simeq 3.3$ . On the other hand, in the case of the coupling between DM and  $Z$ -boson pairs  $g_{ZZ}$ , the dependence on  $s_w$  and  $c_w$  is reversed compared to  $g_{AA}$ . These properties explain why the limit on the new-physics scale  $\Lambda$  from mono-photon ( $\cancel{E}_T + Z (\rightarrow \ell^+ \ell^-)$ ,  $\cancel{E}_T + W/Z (\rightarrow \text{hadrons})$ , mono-jet and VBF  $h \rightarrow \text{invisible}$ ) searches is stronger (weaker) in the upper panel than in the lower panel of Fig. 2.

A second important feature worth noting is that channels with leptons in the final state typically lead to weaker restrictions on the parameter space than modes involving hadrons. This is a simple consequence of the fact that the

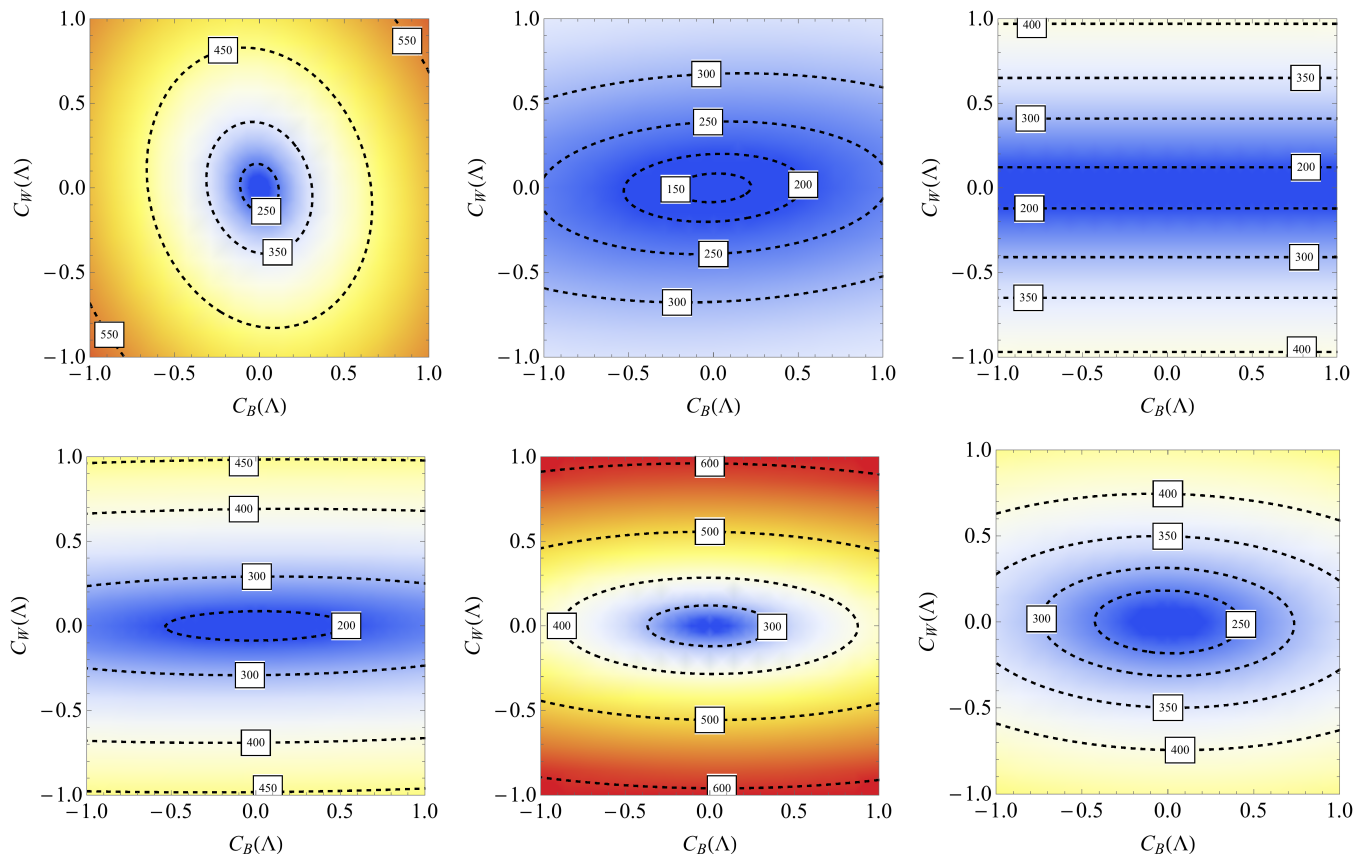


FIG. 3: Limits on  $\Lambda$  in the  $C_B(\Lambda)$ – $C_W(\Lambda)$  plane. The different panels correspond to the mono-photon (upper left),  $\cancel{E}_T + Z \rightarrow \ell^+ \ell^-$  (upper middle),  $\cancel{E}_T + W \rightarrow \mu \nu_\mu$  (upper right),  $\cancel{E}_T + W/Z \rightarrow \text{hadrons}$  (lower left), mono-jet (lower middle) and VBF  $h \rightarrow \text{invisible}$  (lower right) search. All results employ  $m_\chi = 100$  GeV and  $C_{\bar{B}}(\Lambda) = C_{\bar{W}}(\Lambda) = 0$ . The contour labels indicate the value of the new-physics scale in units of GeV.

electroweak SM gauge bosons dominantly decay hadronically. Numerically, one has  $\text{Br}(Z \rightarrow \ell^+ \ell^-) \simeq 7\%$  and  $\text{Br}(W \rightarrow \mu \nu_\mu) \simeq 11\%$ , while  $\text{Br}(Z \rightarrow \text{hadrons}) \simeq 70\%$  and  $\text{Br}(W \rightarrow \text{hadrons}) \simeq 68\%$  [36]. The strong suppression of the leptonic decay widths overcompensates the higher detection efficiencies of final states involving leptons, and as a result the LHC searches for  $\cancel{E}_T + \text{hadrons}$  are superior to those looking for  $\cancel{E}_T + \text{leptons}$  signals.

Our third observation is that the latest mono-jet data are evidently more constraining than the recent VBF  $h \rightarrow \text{invisible}$  search. While these analyses explore the same final state, i.e.  $\cancel{E}_T + 2j$ , they probe quite different parts of the phase space. In fact, the selection criterion that has the biggest impact in our study is the rather loose missing transverse energy cut of  $\cancel{E}_T > 130$  GeV imposed in the VBF  $h \rightarrow \text{invisible}$  search. This selection is tailored for a Higgs boson of 125 GeV, but fares less well if one tries to probe higher-dimensional operators of the form (2). Since the operators  $O_B$  ( $O_{\bar{B}}$ ) and  $O_W$  ( $O_{\bar{W}}$ ) produce a rather hard  $\cancel{E}_T$  spectrum, more severe  $\cancel{E}_T$  requirements allow for a cleaner separation between signal and SM background.

## B. Dependence on two Wilson coefficients

Until now we have studied the constraints on the new-physics scale  $\Lambda$  as a function of the DM mass  $m_\chi$ , keeping the values of the high-scale Wilson coefficients fixed. In the panels of Fig. 3 we instead show contours of constant  $\Lambda$  in the  $C_B(\Lambda)$ – $C_W(\Lambda)$  plane. In all plots we employ  $m_\chi = 100$  GeV and set  $C_{\bar{B}}(\Lambda) = C_{\bar{W}}(\Lambda) = 0$ . The first noticeable feature of the shown predictions is that only the mono-photon signal depends more strongly on  $C_B(\Lambda)$  than  $C_W(\Lambda)$ , while for all the other  $\cancel{E}_T$  channels the situation is reversed. Second, with the exception of the mono-photon case, one observes that the major axes of the elliptic contours in all panels are almost aligned with the  $C_W(\Lambda)$  axes. This means that interference effects between contributions arising from  $O_B$  and  $O_W$  are small in all of these cases. The third important property following from the colour shading of the depicted results is that currently either the newest mono-photon or the mono-jet data provide the leading bounds in the entire  $C_B(\Lambda)$ – $C_W(\Lambda)$  plane. This feature is further illustrated by the upper panel in Fig. 4. In this plot the overlaid numbers indicate the search strategy that

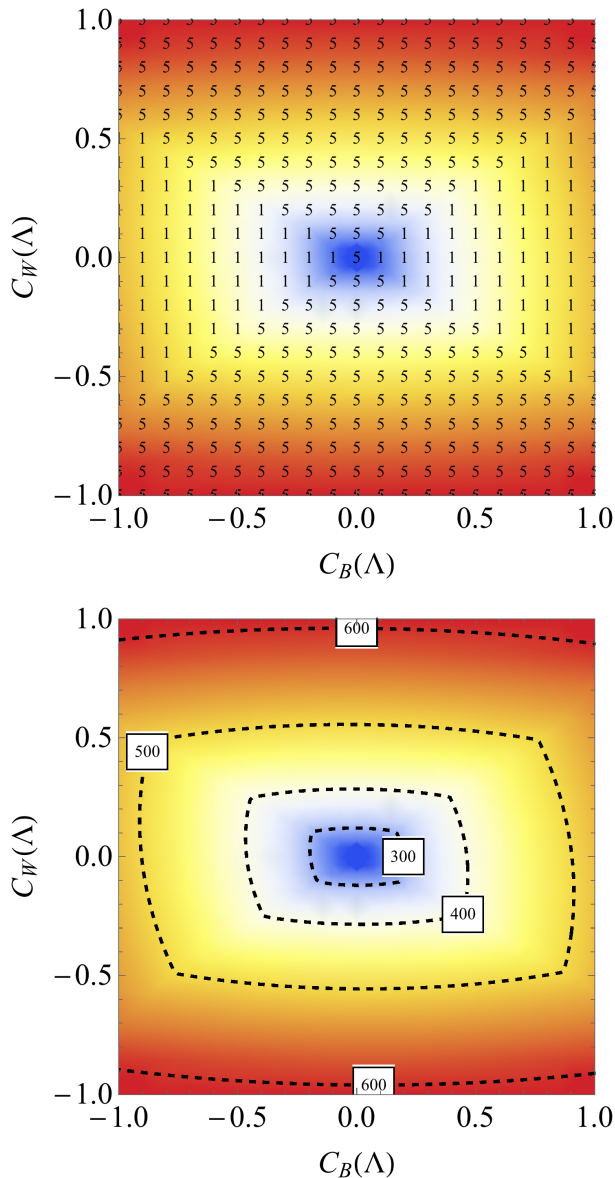


FIG. 4: Combination of the bounds on the new-physics scale in the  $C_B(\Lambda)$ - $C_W(\Lambda)$  plane, employing  $m_\chi = 100$  GeV and  $C_{\tilde{B}}(\Lambda) = C_{\tilde{W}}(\Lambda) = 0$ . In the upper panel the search strategy that provides the leading constraint is indicated by the superimposed numbers, with 1 (5) representing the latest mono-photon (mono-jet) search, while the lower panel shows the resulting contours of constant  $\Lambda$  in units of GeV.

contributes the best sensitivity on  $\Lambda$  at each point, with 1 and 5 corresponding to the mono-photon and mono-jet channel, respectively. One sees that if the ratio of Wilson coefficients satisfies  $|C_B(\Lambda)/C_W(\Lambda)| \gtrsim 1.5$  then the limit (4) gives rise to the strongest constraint, while in the remaining  $C_B(\Lambda)$ - $C_W(\Lambda)$  plane the bound (14) is most restrictive. The  $\Lambda$  contours obtained by combining all available  $\cancel{E}_T$  channels are depicted in the lower panel of Fig. 4.

Finally, we note that the values of  $\Lambda$  that can be excluded with the current data are low compared to typical LHC energies. In order to go beyond the EFT description, one has to specify a ultraviolet (UV) completion, where the operators in (4) arise from a renormalisable theory after integrating out the heavy degrees of freedom mediating the interactions. UV-complete models that generate the operators  $O_B$  and  $O_W$  through loops of states charged under  $U(1)_Y$  and/or  $SU(2)_L$  have been proposed in [3] and their LHC signatures have been studied in [4]. If these new charged particles are light, the high- $p_T$  gauge bosons that participate in the  $\cancel{E}_T$  processes considered here are able to resolve the substructure of the loops. This generically suppresses the cross sections compared to the EFT predictions [33], and thus will weaken the bounds on the interaction strengths of DM and the electroweak gauge bosons to some extent. Furthermore, the light charged mediators may be produced on-shell in  $pp$  collisions, rendering direct LHC searches potentially more restrictive than  $\cancel{E}_T$  searches. Making the above statements precise would require a study of a concrete UV completion.

### C. Future sensitivity

It is also interesting to explore how the reach on the new-physics scale  $\Lambda$  might improve at the 14 TeV LHC. In what follows, we will only consider the mono-jet signal, applying the event selection criteria that have been used in the sensitivity study by ATLAS [37]. These read

$$\begin{aligned}
 p_{T,j_1} &> 300 \text{ GeV}, & |\eta_{j_1}| &< 2.0, \\
 p_{T,j_2} &> 50 \text{ GeV}, & |\eta_{j_2}| &< 3.6, \\
 \Delta\phi_j \cancel{E}_T &> 0.5,
 \end{aligned} \tag{17}$$

and jets are reconstructed using an anti- $k_t$  algorithm with  $R = 0.4$ . Events with a third jet of  $p_{T,j_3} > 50$  GeV and  $|\eta_{j_3}| < 3.6$  are vetoed and the missing transverse energy cut that we employ is  $\cancel{E}_T > 800$  GeV. Note that compared to (11) the  $p_{T,j_1}$ ,  $p_{T,j_2}$  and  $\cancel{E}_T$  thresholds are increased both to avoid pile-up and to enhance the signal-over-background ratio. In order to determine the limits on the scale  $\Lambda$ , we take  $\sigma_{\text{fid}}(pp \rightarrow Z(\rightarrow \bar{\nu}\nu) + j) = 5.5$  fb [37], assuming a total systematic uncertainty on the SM background of 5%. For the choice  $C_B(\Lambda) = 0$ ,  $C_W(\Lambda) = 1$  and  $C_{\tilde{B}}(\Lambda) = C_{\tilde{W}}(\Lambda) = 0$ , we find that with  $25 \text{ fb}^{-1}$  of data, corresponding to the first year of running after the LHC upgrade to 14 TeV, one may be able to set a 95% CL bound of  $\Lambda \gtrsim 1.3$  TeV for  $m_\chi \lesssim 100$  GeV. Compared to the present limit, this corresponds to an improvement of the bound on  $\Lambda$  by more than a factor of 2. With  $300 \text{ fb}^{-1}$  and  $3000 \text{ fb}^{-1}$  of accumulated data, we obtain instead  $\Lambda \gtrsim 1.4$  TeV. These numbers make clear that at 14 TeV the sensitivity of  $\cancel{E}_T + j$  searches will rather soon be limited by systematic uncertainties associated to the irreducible SM background. To what

extent this limitation can be evaded by an optimisation of the mono-jet searches and/or an improved understanding of the  $pp \rightarrow Z (\rightarrow \bar{\nu}\nu) + j$  channel, would require a dedicated study. Such an analysis is beyond the scope of this work.

#### D. Analysis of jet-jet angular correlations

So far we have analysed only observables that are insensitive to whether the  $\cancel{E}_T$  signal is generated by an insertion of the effective operator  $O_B$  ( $O_W$ ) or  $O_{\tilde{B}}$  ( $O_{\tilde{W}}$ ). This ambiguity can however be resolved by measuring the azimuthal angle difference  $\Delta\phi_{j_1 j_2}$  of forward jets produced in  $\cancel{E}_T + 2j$  events [9, 21]. Besides the cuts (17), we impose the following VBF-like selection requirements in our analysis

$$\eta_{j_1} \cdot \eta_{j_2} < 0, \quad \Delta\eta_{j_1 j_2} > 2, \quad m_{j_1 j_2} > 1100 \text{ GeV}. \quad (18)$$

Here the cut on the pseudorapidity separation helps to sculpt the angular correlations between the tagging jets, while the di-jet invariant mass threshold improves the signal-over-background ratio.

In order to understand why the operators  $O_B$  ( $O_W$ ) and  $O_{\tilde{B}}$  ( $O_{\tilde{W}}$ ) lead to different jet-jet angular correlations, one has to consider their Feynman rules. In the case of the operators containing regular field strength tensors this has already been done in (15), while for their dual counterparts we obtain

$$\frac{2i}{\Lambda^3} g_{V_1 V_2} \epsilon^{\mu_1 \mu_2 \nu \lambda} (p_{1\nu} p_{2\lambda} - p_{1\lambda} p_{2\nu}), \quad (19)$$

with  $g_{V_i V_j}$  given in (16). The selection cuts (18) emphasise the parts of the phase space where the external partons experience only a small energy loss and the momentum components of the tagging jets in the beam direction are much greater than those in the transverse plane. In this limit the structure of the  $pp \rightarrow \cancel{E}_T + 2j$  matrix elements is straightforward to work out [38]. In the case of the effective operator  $O_W$ , one gets for instance  $\mathcal{M}_W \sim J_1^{\mu_1} J_2^{\mu_2} (g_{\mu_1 \mu_2} p_1 \cdot p_2 - p_{1\mu_1} p_{2\mu_2}) \sim \vec{p}_{T,j_1} \cdot \vec{p}_{T,j_2}$ , while for  $O_{\tilde{W}}$  one arrives instead at  $\mathcal{M}_{\tilde{W}} \sim \epsilon_{\mu_1 \mu_2 \nu \lambda} J_1^{\mu_1} J_2^{\mu_2} p_1^\nu p_2^\lambda \sim \vec{p}_{T,j_1} \times \vec{p}_{T,j_2}$ . Here  $J_i$  and  $p_i$  denote the currents and momenta of the electroweak gauge bosons that partake in the scattering. These simple arguments imply that the  $\Delta\phi_{j_1 j_2}$  spectrum corresponding to  $O_W$  should be enhanced for collinear tagging jets,  $\Delta\phi_{j_1 j_2} = 0$ , while for  $\Delta\phi_{j_1 j_2} = \pi/2$  it should show an approximate zero. In the case of  $O_{\tilde{W}}$ , on the other hand, the  $\Delta\phi_{j_1 j_2}$  distribution should have a dip if the two jets are collinear,  $\Delta\phi_{j_1 j_2} = 0$ , or back-to-back,  $\Delta\phi_{j_1 j_2} = \pi$ . Note that the above arguments do not depend on the chirality of the DM current. This means that  $O_B$ ,  $O_W$ ,  $O_{\tilde{B}}$ ,  $O_{\tilde{W}}$  and the operators obtained from (2) by replacing  $\bar{\chi}\chi$  with  $\bar{\chi}\gamma_5\chi$  lead to very similar jet-jet angular correlations, as we have explicitly verified.

In Fig. 5 we plot the  $\Delta\phi_{j_1 j_2}$  spectra for the choices  $C_B(\Lambda) = 0$ ,  $C_W(\Lambda) = 1$  (red curve) and  $C_{\tilde{B}}(\Lambda) = 0$ ,

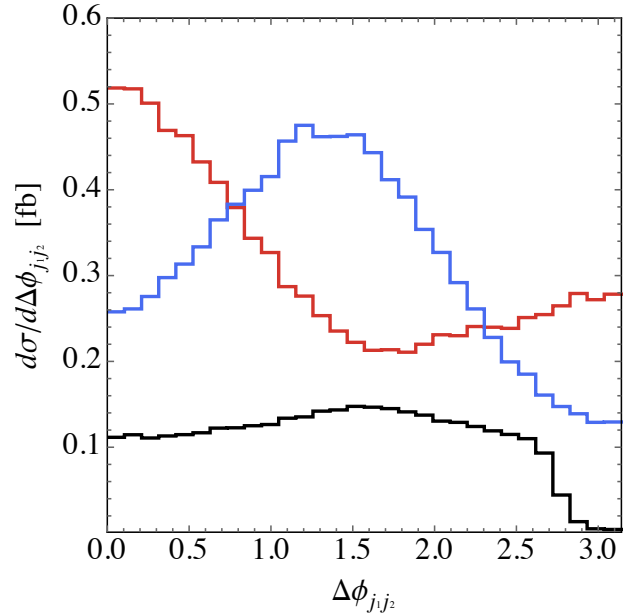


FIG. 5: Azimuthal angle distributions at the 14 TeV LHC. The signal curves correspond to  $C_B(\Lambda) = 0$ ,  $C_W(\Lambda) = 1$  (red) and  $C_{\tilde{B}}(\Lambda) = 0$ ,  $C_{\tilde{W}}(\Lambda) = 1$  (blue), and both use  $\Lambda = 1 \text{ TeV}$  and  $m_\chi = 100 \text{ GeV}$ . For comparison the prediction of the dominant SM background process  $pp \rightarrow Z (\rightarrow \bar{\nu}\nu) + 2j$  (black) employing the same event selection criteria is shown as well.

$C_{\tilde{W}}(\Lambda) = 1$  (blue curve). All shown predictions are obtained for the 14 TeV LHC and employ  $\Lambda = 1 \text{ TeV}$  and  $m_\chi = 100 \text{ GeV}$ . The fiducial signal cross sections amount to 1.0 fb, independently of whether the insertion of  $O_W$  or  $O_{\tilde{W}}$  is considered. The expected sine-like (cosine-like) behaviour of the modulation in the azimuthal angle distribution corresponding to  $O_W$  ( $O_{\tilde{W}}$ ) is clearly visible in the figure. These shapes should be contrasted with the spectrum of the dominant SM background process  $pp \rightarrow Z (\rightarrow \bar{\nu}\nu) + 2j$  (black curve), which is rather flat for values  $\Delta\phi_{j_1 j_2} \lesssim 2.6$  and then rapidly drops to zero. The corresponding fiducial cross section is 0.35 fb, implying a signal-over-background ratio of  $S/\sqrt{B} \simeq 8.4$ , 29 and 93 for  $25 \text{ fb}^{-1}$ ,  $300 \text{ fb}^{-1}$  and  $3000 \text{ fb}^{-1}$  of data, respectively.

The given  $S/\sqrt{B}$  values imply that running the LHC for a couple of years at 14 TeV should provide a sufficient number of events to analyse the jet-jet angular correlations. To quantify this statement, we use a toy MC and generate event samples for both signals and background corresponding to  $300 \text{ fb}^{-1}$  and  $3000 \text{ fb}^{-1}$  of luminosity. The resulting differential cross sections are then fitted to [39]

$$\frac{1}{\sigma} \frac{d\sigma}{d\Delta\phi_{j_1 j_2}} = \sum_{n=0}^2 a_n \cos(n\Delta\phi_{j_1 j_2}). \quad (20)$$

The coefficient  $a_0$  is fixed by the normalisation of the  $\Delta\phi_{j_1 j_2}$  spectrum, and the ratio  $r_1 = a_1/a_0$  turns out to be rather insensitive to which type of higher-dimensional

interactions is considered. In contrast, the combination  $r_2 = a_2/a_0$  is a measure of the CP nature of the interactions that lead to the  $2j$  final state (see e.g. [38, 39]). This ratio is expected to be positive (negative) for an insertion of  $O_B$  ( $O_{\bar{B}}$ ) and  $O_W$  ( $O_{\bar{W}}$ ). We stress that by considering normalised  $\Delta\phi_{j_1j_2}$  distributions, theoretical uncertainties are reduced and that the predictions become fairly independent of EFT assumptions [21].

In Fig. 6 we present the results of our toy MC. The upper panel (lower panel) corresponds to  $300\text{ fb}^{-1}$  ( $3000\text{ fb}^{-1}$ ) of LHC data collected at 14 TeV. The expected azimuthal angle distributions for the signal plus background predictions are coloured blue (red) for  $O_W$  ( $O_{\bar{W}}$ ). For comparison, the SM-only result (grey) divided by a factor of 3 is also shown. The solid curves illustrate the best fits to (20), restricting the rapidity separation  $\Delta\phi_{j_1j_2}$  to the range  $[0, 2.5]$ . For  $300\text{ fb}^{-1}$  of data, we obtain for  $r_2$  the central values and uncertainties

$$\begin{aligned} (r_2)_{W+\text{SM}} &= 0.15 \pm 0.10, \\ (r_2)_{\bar{W}+\text{SM}} &= -0.45 \pm 0.14, \\ (r_2)_{\text{SM}} &= -0.12 \pm 0.22. \end{aligned} \quad (21)$$

In the case of  $3000\text{ fb}^{-1}$  of luminosity, we find instead

$$\begin{aligned} (r_2)_{W+\text{SM}} &= 0.18 \pm 0.03, \\ (r_2)_{\bar{W}+\text{SM}} &= -0.40 \pm 0.04, \\ (r_2)_{\text{SM}} &= -0.13 \pm 0.07. \end{aligned} \quad (22)$$

We observe that for  $O_W$  ( $O_{\bar{W}}$ ) the combination  $r_2$  is indeed positive (negative). Defining a significance as  $s_k = ((r_2)_{k+\text{SM}} - (r_2)_{\text{SM}})/(\Delta r_2)_{k+\text{SM}}$ , we get from (21) the values  $s_W = 2.7$  and  $s_{\bar{W}} = -2.4$ , while (22) leads to  $s_W = 10.3$  and  $s_{\bar{W}} = -6.8$ . Our toy MC study corresponding to  $300\text{ fb}^{-1}$  ( $3000\text{ fb}^{-1}$ ) of data hence suggest that a distinction between the azimuthal angle distributions of  $O_W$  and  $O_{\bar{W}}$  at the  $5\sigma$  ( $17\sigma$ ) level should be possible at the 14 TeV LHC. We emphasise that our toy study assumes a perfect detector and that we have not optimised the cuts (18) to achieve the best significance. Once the data is on tape, it will become an experimental issue of how stringent the VBF-like selections can be made to extract the most information on the jet-jet angular correlations for a given limited sample size.

#### IV. CONCLUSIONS

In this article we have studied LHC constraints on effective dimension-7 operators that couple DM to the SM electroweak gauge bosons and emphasised the complementarity of different  $\cancel{E}_T$  searches for constraining the associated Wilson coefficients. Focusing on the interactions that induce only velocity-suppressed annihilation rates, we have combined the information on all individual search modes that are available after LHC run-1. In this

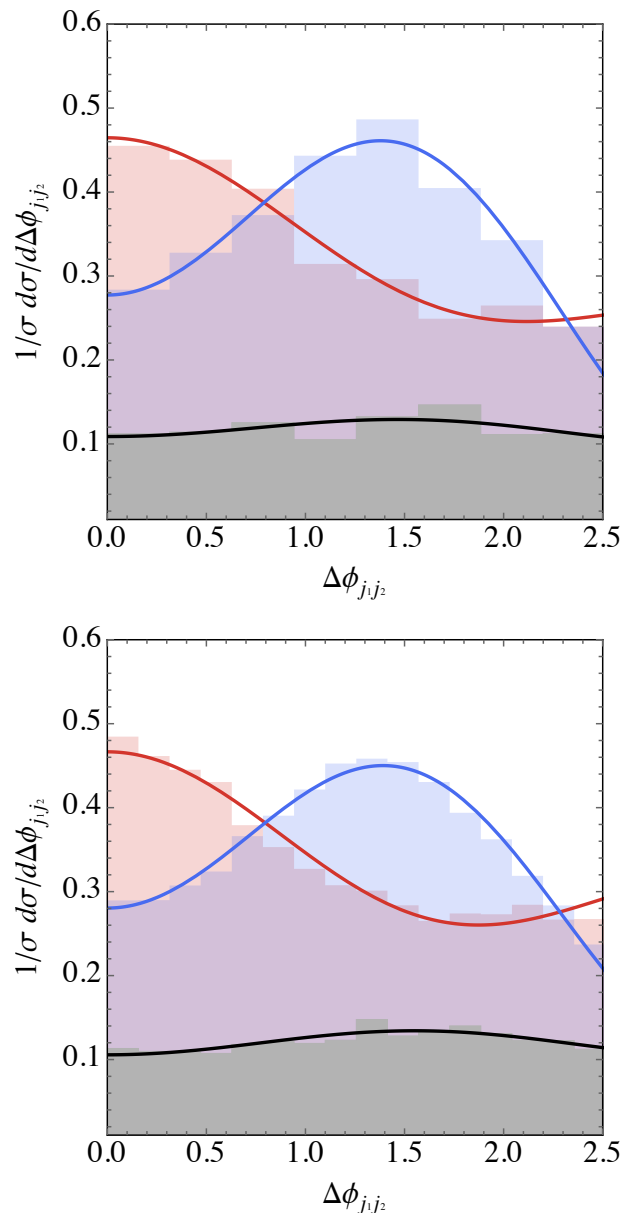


FIG. 6: Normalised  $\Delta\phi_{j_1j_2}$  distributions for  $300\text{ fb}^{-1}$  (upper panel) and  $3000\text{ fb}^{-1}$  (lower panel) of 14 TeV LHC data. The red (blue) histogram shows the signal plus background prediction for  $O_W$  ( $O_{\bar{W}}$ ). The grey bar chart represents the expected SM background, which for better visibility, has been rescaled by a factor of  $1/3$ . The solid curves indicate the best fits of the form  $a_0 + a_1 \cos \Delta\phi_{j_1j_2} + a_2 \cos(2\Delta\phi_{j_1j_2})$ . See text for additional explanations.

way we are able to derive bounds on the new-physics scale  $\Lambda$  that exceed all previous limits. Our studies show that at present, depending on the choice of parameters, either mono-photon or mono-jet searches provide the most severe constraints on the considered dimension-7 interactions. For DM masses  $m_\chi \lesssim 100\text{ GeV}$  and Wilson coefficients  $|C_k(\Lambda)| \simeq 1$ , the existing 8 TeV LHC searches



allow to exclude values of  $\Lambda$  below about 600 GeV at 95% CL. The improved reach of  $\cancel{E}_T$  analyses in 2015 and beyond is also studied, finding that with  $25 \text{ fb}^{-1}$  of 14 TeV data, LHC mono-jet searches should be able to improve the latter bound to approximately 1.3 TeV. Beyond this point further progress will be hindered by the imperfect understanding of irreducible SM backgrounds such as  $pp \rightarrow Z (\rightarrow \bar{\nu}\nu) + j$ . Finding ways to overcome these limitations will be crucial to exploit the full physics potential of  $\cancel{E}_T$  searches to be carried out at later stages of the LHC.

We have furthermore emphasised that given the large statistics expected at the phase-1 and phase-2 upgrades of the 14 TeV LHC,  $\cancel{E}_T$  searches should be able to not only determine integrated, but also differential cross sections. From the theoretical point of view, such normalised distributions have the clear advantage, that compared to the total cross sections theoretical uncertainties are reduced and that the obtained predictions depend only weakly on the assumptions underlying the EFT description. As an example we have explored the prospects to measure jet-jet angular correlations in  $\cancel{E}_T + 2j$  events. Taking into account the pseudorapidity correlations of the two tagging jets, the resulting distributions in the azimuthal angle separation  $\Delta\phi_{j_1 j_2}$  exhibit the relative strength of CP-even and CP-odd interactions of DM with gauge boson pairs. Our toy MC studies indicate that already with  $300 \text{ fb}^{-1}$  of data a distinction between the

new-physics and the SM-only hypotheses can be achieved at a statistically significant level, and that the sensitivity of the discussed searches is greatly improved by going to  $3000 \text{ fb}^{-1}$  of luminosity. A more precise determination of the analysing power, including systematic uncertainties would require a full detector simulation, which is beyond the scope of the present article. We however believe that it is imperative that the ATLAS and CMS collaborations direct some activity towards the study of differential distributions of final states like  $\cancel{E}_T + 2j$ .

### Acknowledgments

We thank Tim Tait for clarifying discussions concerning his work [10] and are grateful to Benjamin Fuks, Emanuele Re and Giulia Zanderighi for help with MadGraph and/or PYTHIA. AC is supported by a Marie Curie Intra-European Fellowship of the European Community's 7<sup>th</sup> Framework Programme under contract number PIEF-GA-2012-326948. UH acknowledges the hospitality and support of the CERN theory division and the Munich Institute for Astro- and Particle Physics (MIAPP) of the DFG cluster of excellence "Origin and Structure of the Universe". The research of AH is supported by an STFC Postgraduate Studentship.

- 
- [1] A. Askew, S. Chauhan, B. Penning, W. Shepherd and M. Tripathi, *Int. J. Mod. Phys. A* **29**, 1430041 (2014) [arXiv:1406.5662 [hep-ph]].
- [2] N. Weiner and I. Yavin, *Phys. Rev. D* **86**, 075021 (2012) [arXiv:1206.2910 [hep-ph]].
- [3] N. Weiner and I. Yavin, *Phys. Rev. D* **87**, 023523 (2013) [arXiv:1209.1093 [hep-ph]].
- [4] J. Liu, B. Shuve, N. Weiner and I. Yavin, *JHEP* **1307**, 144 (2013) [arXiv:1303.4404 [hep-ph]].
- [5] A. Rajaraman, T. M. P. Tait and D. Whiteson, *JCAP* **1209**, 003 (2012) [arXiv:1205.4723 [hep-ph]].
- [6] M. T. Frandsen, U. Haisch, F. Kahlhoefer, P. Mertsch and K. Schmidt-Hoberg, *JCAP* **1210**, 033 (2012) [arXiv:1207.3971 [hep-ph]].
- [7] A. Rajaraman, T. M. P. Tait and A. M. Wijangco, *Phys. Dark Univ.* **2**, 17 (2013) [arXiv:1211.7061 [hep-ph]].
- [8] A. Crivellin and U. Haisch, *Phys. Rev. D* **90**, 115011 (2014) [arXiv:1408.5046 [hep-ph]].
- [9] R. C. Cotta, J. L. Hewett, M. P. Le and T. G. Rizzo, *Phys. Rev. D* **88** (2013) 116009 [arXiv:1210.0525 [hep-ph]].
- [10] L. M. Carpenter, A. Nelson, C. Shimmin, T. M. P. Tait and D. Whiteson, *Phys. Rev. D* **87**, 074005 (2013) [arXiv:1212.3352].
- [11] G. Aad *et al.* [ATLAS Collaboration], *Phys. Rev. D* **90**, 012004 (2014) [arXiv:1404.0051 [hep-ex]].
- [12] A. Nelson, L. M. Carpenter, R. Cotta, A. Johnstone and D. Whiteson, *Phys. Rev. D* **89**, 056011 (2014) [arXiv:1307.5064 [hep-ph]].
- [13] N. Lopez, L. M. Carpenter, R. Cotta, M. Frate, N. Zhou and D. Whiteson, *Phys. Rev. D* **89**, 115013 (2014) [arXiv:1403.6734 [hep-ph]].
- [14] V. Khachatryan *et al.* [CMS Collaboration], arXiv:1410.8812 [hep-ex].
- [15] G. Aad *et al.* [ATLAS Collaboration], *Phys. Rev. D* **91**, 012008 (2015) [arXiv:1411.1559 [hep-ex]].
- [16] G. Aad *et al.* [ATLAS Collaboration], *Phys. Rev. Lett.* **112**, 041802 (2014) [arXiv:1309.4017 [hep-ex]].
- [17] S. Chatrchyan *et al.* [CMS Collaboration], *Eur. Phys. J. C* **74**, 2980 (2014) [arXiv:1404.1344 [hep-ex]].
- [18] G. Aad *et al.* [ATLAS Collaboration], *JHEP* **1409**, 037 (2014) [arXiv:1407.7494 [hep-ex]].
- [19] V. Khachatryan *et al.* [CMS Collaboration], arXiv:1408.2745 [hep-ex].
- [20] V. Khachatryan *et al.* [CMS Collaboration], arXiv:1408.3583 [hep-ex].
- [21] U. Haisch, A. Hibbs and E. Re, *Phys. Rev. D* **89**, 034009 (2014) [arXiv:1311.7131 [hep-ph]].
- [22] Y. L. Dokshitzer, G. D. Leder, S. Moretti and B. R. Webber, *JHEP* **9708**, 001 (1997) [hep-ph/9707323].
- [23] J. M. Butterworth, A. R. Davison, M. Rubin and G. P. Salam, *Phys. Rev. Lett.* **100**, 242001 (2008) [arXiv:0802.2470 [hep-ph]].
- [24] M. Cacciari, G. P. Salam and G. Soyez, *JHEP* **0804**, 063 (2008) [arXiv:0802.1189 [hep-ph]].
- [25] J. de Favereau *et al.* [DELPHES 3 Collaboration], *JHEP* **1402**, 057 (2014) [arXiv:1307.6346 [hep-ex]].
- [26] U. Haisch, F. Kahlhoefer and E. Re, *JHEP* **1312**, 007

- (2013) [arXiv:1310.4491 [hep-ph]].
- [27] N. D. Christensen and C. Duhr, *Comput. Phys. Commun.* **180**, 1614 (2009) [arXiv:0806.4194 [hep-ph]].
- [28] C. Degrande, C. Duhr, B. Fuks, D. Grellscheid, O. Mattelaer and T. Reiter, *Comput. Phys. Commun.* **183**, 1201 (2012) [arXiv:1108.2040 [hep-ph]].
- [29] J. Alwall, M. Herquet, F. Maltoni, O. Mattelaer and T. Stelzer, *JHEP* **1106**, 128 (2011) [arXiv:1106.0522 [hep-ph]].
- [30] J. Pumplin, D. R. Stump, J. Huston, H. L. Lai, P. M. Nadolsky and W. K. Tung, *JHEP* **0207**, 012 (2002) [hep-ph/0201195].
- [31] T. Sjostrand, S. Mrenna and P. Z. Skands, *Comput. Phys. Commun.* **178**, 852 (2008) [arXiv:0710.3820 [hep-ph]].
- [32] M. Cacciari, G. P. Salam and G. Soyez, *Eur. Phys. J. C* **72**, 1896 (2012) [arXiv:1111.6097 [hep-ph]].
- [33] U. Haisch, F. Kahlhoefer and J. Unwin, *JHEP* **1307**, 125 (2013) [arXiv:1208.4605 [hep-ph]].
- [34] U. Haisch and F. Kahlhoefer, *JCAP* **1304**, 050 (2013) [arXiv:1302.4454 [hep-ph]].
- [35] U. Haisch and E. Re, arXiv:1503.00691 [hep-ph].
- [36] K. A. Olive *et al.* [Particle Data Group Collaboration], *Chin. Phys. C* **38**, 090001 (2014).
- [37] ATLAS Collaboration, <http://cds.cern.ch/record/1708859/files/ATL-COM-PHYS-2014-549.pdf>
- [38] T. Plehn, D. L. Rainwater and D. Zeppenfeld, *Phys. Rev. Lett.* **88**, 051801 (2002) [hep-ph/0105325].
- [39] V. Hankele, G. Klamke and D. Zeppenfeld, hep-ph/0605117.